Hydrol. Earth Syst. Sci. Discuss., https://doi.org/10.5194/hess-2017-757
Manuscript under review for journal Hydrol. Earth Syst. Sci.
Discussion started: 24 January 2018

Hydrology and Earth System Sciences
Open Access
Discussions

Global 5-km resolution estimates of secondary evaporation including irrigation through satellite data assimilation

Albert I.J.M. van Dijk[1], Jaap Schellekens[2,3], Marta Yebra[1], Hylke E. Beck[4], Luigi J. Renzullo[1], Albrecht Weerts[2,5], Gennadii Donchyts[2]

[1] Fenner School of Environment & Society, Australian National University, Canberra, ACT, Australia

[2] Deltares, Delft, The Netherlands

[3] Vandersat B.V., Haarlem, The Netherlands

[4] Princeton University, Princeton, NJ, USA

[5] Wageningen University & Research, Wageningen, The Netherlands

Hydrol. Earth Syst. Sci. Discuss., https://doi.org/10.5194/hess-2017-757
Manuscript under review for journal Hydrol. Earth Syst. Sci.
Discussion started: 24 January 2018

Hydrology and Earth System Sciences
Open Access
Discussions

Abstract

A portion of globally generated surface and groundwater resources evaporates from wetlands, water bodies and irrigated areas. This secondary evaporation of 'blue' water directly affects the remaining water resources available for ecosystems and human use. At the global scale, a lack of detailed water balance studies and direct observations limits our understanding of the magnitude and spatial and temporal distribution of secondary evaporation. Here, we propose a methodology to assimilate satellite-derived information into the landscape hydrological model W3 at an unprecedented 0.05° or c. 5 km resolution globally. The assimilated data are all derived from MODIS observations, including surface water extent, surface albedo, vegetation cover, leaf area index, canopy conductance, and land surface temperature (LST). The information from these products is imparted on the model in a simple but efficient manner, through a combination of direct insertion of surface water extent, evaporation flux adjustment based on LST, and parameter nudging for the other observations. The resulting water balance estimates were evaluated against river basin discharge records and the water balance of closed basins and demonstrably improved water balance estimates compared to ignoring secondary evaporation (e.g., bias improved from +38 mm/d to +2 mm/d). The evaporation estimates derived from assimilation were combined with global mapping of irrigation crops to derive a minimum estimate of irrigation water requirements (I_0), representative of optimal irrigation efficiency. Our I_0 estimates were lower than published country-level estimates of irrigation water use produced by alternative estimation methods, for reasons that are discussed. We estimate that 16% of globally generated water resources evaporate before reaching the oceans, enhancing total terrestrial evaporation by $6.1 \cdot 10^{12}$ m^3 y^{-1} or 8.8%. Of this volume, 5% is evaporated from irrigation areas, 58% from terrestrial water bodies and 37% from other surfaces. Model-data assimilation at even higher spatial resolutions can achieve a further reduction in uncertainty but will require more accurate and detailed mapping of surface water dynamics and areas equipped for irrigation.

Introduction

The generation of surface and groundwater resources is commonly conceptualised one-dimensionally as the net difference between precipitation, evaporation (including transpiration) and soil storage change. However, some part of the generated 'blue' water (Falkenmark and Rockström, 2004) subsequently inundates floodplains, accumulates in wetlands and freshwater bodies, or is extracted for irrigation. A fraction of that water will evaporate in this second instance. This 'secondary evaporation' directly reduces the remaining blue water resources available for ecosystems and economic uses downstream but also increases the use of water by terrestrial ecosystems before discharging into the oceans. At the global scale, our understanding of the magnitude and spatiotemporal distribution of secondary evaporation is limited by a lack of detailed water balance studies and direct observations. Until recently, land surface models ignore lateral water transport and secondary evaporation altogether or provide a rudimentary description. This is understandable, given the complexity and computational challenge in simulating the lateral redistribution and secondary evaporation of water at the global scale. However, it is increasingly clear that the lateral redistribution of water cannot be ignored in global water resources analyses (Oki and Kanae, 2006; Alcamo et al., 2003), carbon cycle analysis (Melton et al., 2013) and regional and global climate studies (e.g., Thiery et al., 2017).

Even approximate numbers on the importance of secondary evaporation in the global water cycle are not available. Oki and Kanae (2006) derived global bulk estimates of gross evaporation from lakes, wetlands and irrigation (combined $10.1 \cdot 10^{12}$ m^3 y^{-1}) but their estimate was based on modelling only and included both primary and secondary evaporation. There have been some studies estimating irrigation water requirements at the global scale (Döll and Siebert, 2002; Wada et al., 2014; Siebert and Döll, 2010) but these studies were based on idealised modelling, did not attempt to separate between primary and secondary evaporation, and did not consider other sources of secondary evaporation.

There have been attempts to use satellite observations to estimate the importance of secondary evaporation at a regional scale. For example, Doody et al. (2017) used MODIS-based evaporation estimates (Guerschman et al., 2009) over Australia to delineate areas receiving lateral inflows. They used ancillary data to attribute these to surface water inundation, irrigation, and groundwater-dependent ecosystems, respectively. At the global scale, Wang-Erlandsson et al. (2016) used satellite-based ET estimates from several sources to infer rooting depth, which provided some insights into the spatial distribution of surface- and groundwater dependent ecosystems.

Historically, three contrasting approaches have been followed to estimate evaporation: water balance modelling; inference from land surface temperature (LST) remote sensing; and estimation based on vegetation remote sensing. All three approaches rely on meteorological data and effectively involve a land surface model of some description, albeit of variable complexity. Hybrids between the three approaches have also been developed over time to mitigate respective weaknesses (Glenn et al., 2011). For example, dynamic simulation of the soil water balance can provide a valuable constraint on satellite-based evaporation estimates in water-limited environments; provided precipitation is the only source of water for evaporation, and accurate precipitation estimates are available (Glenn et al., 2011; Miralles et al., 2016). However, where there are additional sources of water or unexpected soil moisture dynamics, applying this constraint can degrade evaporation estimates.

Beyond dynamic hydrological models, evaporation products based more closely on vegetation remote sensing implicitly account for the effect of lateral water redistribution on transpiration, but often do not account for open water evaporation (Yebra et al., 2013; Zhang et al., 2016), with exceptions (Guerschman et al., 2009; Miralles et al., 2016). Satellite-observed LST has a direct, physical connection to the surface heat balance, and through the overall surface water and energy balance can provide a constraint on evaporation estimates. Several techniques have been developed to infer evaporation from LST, and many successful applications at local scale have been documented (Kalma et al., 2008). Over larger areas, the application of LST-based methods is complicated by the need for time-of-overpass estimates of radiation components, air temperature, and aerodynamic conductance (Kalma et al., 2008; Van Niel et al., 2011). There are promising developments that can overcome some of these challenges (Anderson et al., 2016), although they are yet to be fully evaluated.

Arguably, the most promising approach to evaporation estimation is to combine water balance modelling, LST remote sensing, and vegetation remote sensing within a model-data fusion framework. This prospect motivated the present study.

Aim

Our objective was to develop a methodology to assimilate optical and thermal observations by the MODIS satellite instruments into a 0.05° resolution global hydrological model to estimate evaporation and to evaluate the quality and quantitative accuracy of the resulting estimates as much as possible. Based on the resulting estimates, we wished to answer the following questions:

- What is the magnitude of secondary evaporation of surface and groundwater resources in the global and regional water cycle?
- What is the magnitude of irrigation evaporation and how does it relate to total agricultural water withdrawals?
- What are the contributions of secondary evaporation from irrigation, permanent water bodies, ephemeral water bodies, and other surfaces?
- Is secondary evaporation likely to have a noticeable impact on the global carbon cycle and climate system?

Materials and Methods

Global water balance model description

The World-Wide Water model (W3) version 2 is an evolution of the AWRA-L and W3RA group of models. The AWRA-L model is used operationally for water balance estimation across Australia at 0.05° resolution by the Bureau of Meteorology. An overview of the operational AWRA-L model (version 5) can be found in Frost et al. (2016b), with details on the scientific basis in Van Dijk (2010). Very briefly, the model operates at daily time step and is grid-based. Each cell is conceptualised to represent several parallel small, identical catchments. The soil column is conceptualised as a three-layer unsaturated zone overlaying an unconfined groundwater store. The unsaturated soil water balance and corresponding water and energy fluxes can be simulated separately for hydrological response units (HRUs) that each occupy a fraction of the grid cell. Sub-grid parameterisations are applied to simulate the area fractions with surface water, groundwater saturation and root water access to groundwater dynamically, based on the hypsometric curves (i.e., the cumulative distribution function of elevation) for each grid cell (Peeters et al., 2013).

The W3 (version 2) model is a global implementation of AWRA-L (version 5) at the same 0.05° resolution. Important differences are as follows (details in Appendix A). Separate HRUs were not considered, however, the water balance of permanent water bodies is calculated separately. Global gridded climate time series and surface, vegetation and soil parameterisation data were used. We used the cumulative distribution function of Height Above Nearest Drainage (HAND; Nobre et al., 2015) for each grid cell instead of hypsometric curves, which we derived from high-resolution global digital elevation models. Five model parameters that were both relatively uncertain and influential were calibrated and regionalised using large global data sets of site measurements evaporation and near-surface soil moisture, and a global dataset of catchment streamflow records (the parameters represent proportional adjustments to initial estimates of, respectively, maximum canopy conductance, relative canopy rainfall evaporation rate, soil evaporation, saturated soil conductivity, and soil conductivity decay with depth). Differences less relevant here include the addition of a snow water balance model and grid-based river routing. A range of W3-simulated water and energy balance terms has been made publicly available as part of 'Tier-2' of the eartH2Observe project (Schellekens et al., 2017). The AWRA-L and W3 models have received extensive evaluation, demonstrating realistic estimates of evaporation, soil moisture, deep drainage, streamflow and total water storage (e.g., for more recent implementations, Tian et al., 2017; Frost et al., 2016a; Beck et al., 2016; Holgate et al., 2016).

Data assimilation

All data assimilated here were derived from NASA's Moderate Resolution Imaging Spectroradiometer (MODIS) instruments. The data included albedo, reflectance, leaf area index (LAI) and LST (details in Appendix A). We followed the following steps, except for LST. First, the MODIS band reflectances were used to estimate vegetation cover fraction and canopy conductance following Yebra et al. (2015; 2013); surface water extent was estimated following Van Dijk et al. (2016); and MODIS albedo, snow cover fraction and LAI products were used in their original form. Next, seven model states were updated using a simple nudging scheme. For each state, the observation and model

Hydrol. Earth Syst. Sci. Discuss., https://doi.org/10.5194/hess-2017-757
Manuscript under review for journal Hydrol. Earth Syst. Sci.
Discussion started: 24 January 2018

Hydrology and Earth System Sciences
Open Access
Discussions

error estimates were based on an assessment of the noise in the observational data, the expected dynamic rate of change, and the expected skill of the model. The resulting 'gain' factors (i.e. the relative weight of observations) varied from 0.5 for LAI and snow fraction to 0.99 for surface water fraction. The updated states were also used dynamically to update six related parameters of diagnostic model equations, including a parameter relating vegetation cover fraction to canopy conductance, another relating vegetation cover to LAI, and four parameters relating surface state to albedo.

The approach to assimilate LST observations was different. In this case, the dynamic model was run one timestep forward to produce a background estimate of the surface energy balance and evaporation flux. The corresponding average daytime LST (T_s, K) was estimated from the average daytime sensible heat flux (H, W m^{-2}) as

$$T_s = T_a + \frac{H}{\rho_a c_p g_a} \tag{1}$$

where T_a is air temperature (K), ρ_a air density (kg m^{-3}), c_p specific heat capacity (J kg^{-1} K^{-1}), and $g_a(u)$ aerodynamic conductance (mm s^{-1}). The latter is a function of wind speed scaled by the wind speed measurement and vegetation heights, respectively, following Thom (1975).

Poor characterisation of spatial gradients in radiative exposure, air temperature, and wind speed in areas with relief can cause a poor relationship between observed and modelled LST (Kalma et al., 2008). Fortunately, secondary evaporation primarily occurs in regions with low relief. Therefore, data assimilation was only attempted for areas with an average slope less than 3% (as calculated from the higher resolution DEM; Appendix A). This threshold was empirically found to include a large majority of observed surface water inundation and mapped irrigation areas.

A second challenge relates to the inconsistency between the observation time-of-overpass LST and model-predicted mean daytime LST. We assumed that time-of-overpass and mean daytime LST will have different spatial averages, but share a near-identical spatial pattern of deviations from the spatial averages. This assumption also helps to remove systematic bias, which is the largest source of error in MODIS LST estimates. Previous assessments report errors in MODIS that are within 0.7 K under conducive atmospheric conditions but can increase to 3 or 4 K due to errors in atmospheric correction that tend to cause similar level of bias over a larger area (Wan et al., 2004; Wan, 2008; Wan and Li, 2008; Hulley et al., 2012).

In the assimilation step, the median observed and modelled LST were calculated for all low-relief grid cells within a spatial window of 15° latitude and longitude and subtracted from the respective gridded LST values. Subsequently, we calculated the difference between resulting observed and modelled LST values. The calculated difference was reduced by up to 1 K to conservatively allow for uncertainty in the assumptions and errors in the observations. Next, the model LST was updated with the remaining difference towards the MODIS-observed LST. An updated latent heat flux ($\lambda E'$ in W m^{-2}; the prime indicating the updated variable) can be calculated from the energy balance as

Hydrol. Earth Syst. Sci. Discuss., https://doi.org/10.5194/hess-2017-757
Manuscript under review for journal Hydrol. Earth Syst. Sci.
Discussion started: 24 January 2018

Hydrology and Earth System Sciences
Open Access
Discussions

$$\lambda E' = A - H' = A - \rho_a c_p g_a (T_s{}' - T_a) \quad (2)$$

where A is available energy (W m^{-2}). To ensure physical consistency within the model context, $\lambda E'$ was constrained to positive values below or equal to potential evaporation E_0, calculated following Penman-Monteith theory (details in Van Dijk, 2010). Temporal consistency was ensured by recording the ratio $\lambda E'/\lambda E$ and using it to adjust simulated λE for subsequent days until a new LST observation was available. Finally, E was calculated through division by the latent heat of vaporisation λ.

To illustrate the data assimilation, time series of observations and model results for one 0.05° grid cell in the Nile delta in Egypt are shown in Figure 1. This grid cell was chosen because it represents one of comparatively few grid cells worldwide deemed to be 100% equipped for irrigation in global mapping (although annual maximum NDVI derived from Landsat suggests that only 80–81% of the area is in fact irrigated; Figure 1a). The processing steps are illustrated by a comparison of observed, background and analysis LST estimates for the year 2002 (Figure 1b), and the resulting sensible heat flux (Figure 1c) and daily evaporation (Figure 1d). Corresponding temporal patterns in the evaporative fraction (E/E_0) show that data assimilation brings the temporal pattern of evaporative fraction in close agreement with satellite-observed vegetation cover fraction (Figure 1e), which provides as a largely independent consistency test.

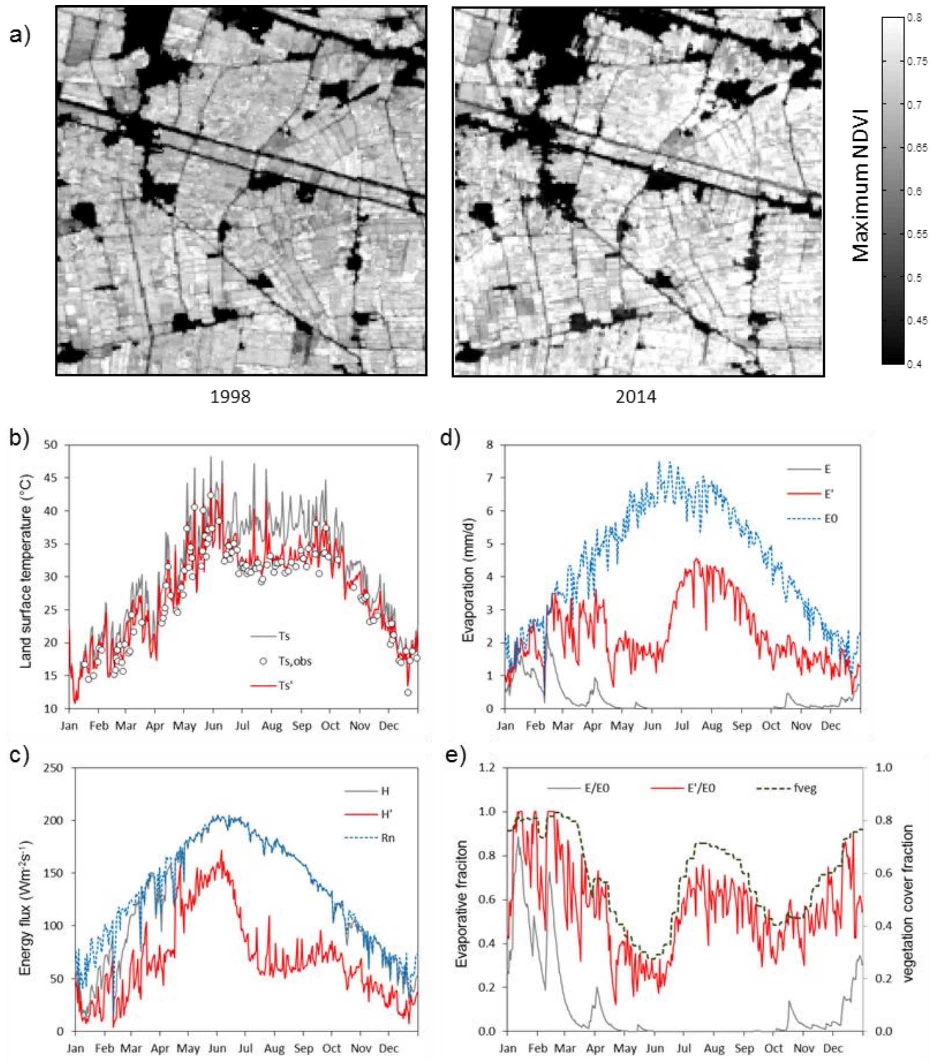

Figure 1. Illustration of method to assimilation MODIS land surface temperature observations. Data shown are for 2002, for 0.05° grid cell in the Nile River delta, Egypt (centred 31.075°N, 30.325°E). (a) *Maximum normalised difference vegetation index* (NDVI) derived from Landsat imagery provided by Google Earth Engine, suggesting that effectively 81% and 80% of the grid cell was cropped in 1998 and 2014, respectively. (b) *Land surface temperature*: background (T_s, grey line), observed ($T_{s,obs}$, circles) and analysis (T_s', red line) estimates for the grid cell with average bias across the 15° window removed. (c) *Sensible heat flux*: background (H, grey) and analysis (H', red) estimates along with net radiation (R_n, blue). (d) *Evaporation*: background (E, grey) and analysis (E', red) estimates along with potential evaporation (E_0, blue). (e) *Evaporative fraction*: background (E/E_0, grey) and analysis (E'/E_0, red) along with vegetation cover fraction derived from MODIS NDVI (f_{veg}, green).

Irrigation water use estimation

For irrigated areas, the long-term average difference between precipitation and total evaporation derived from data assimilation provides an estimate of the importance of additional water inputs. However, it cannot be interpreted directly as an estimate of irrigation water requirements, much less as an estimate of water withdrawals. This is because precipitation and crop water requirements are both unevenly distributed in time, and there is limited water storage capacity in the crop root zone. Additional water is lost from the root zone through drainage and runoff, which will need to be compensated by additional irrigation inputs. This field-level irrigation inefficiency does not necessarily change the long-term net water balance: provided total precipitation and evaporation do not change, the additional inputs will equal the additional runoff and drainage. However, such inefficiencies do need to be accounted for when estimating the total amount of irrigation water required (Siebert and Döll, 2010).

Estimating total field-level irrigation water requirements is sensitive to assumptions about the capacity for added water to remain stored in the root zone irrigation and about strategies (e.g., pursuing a stable low or high soil moisture or paddy water level, suboptimal or soil moisture deficit irrigation, flood irrigation or partial drip irrigation, and so on). Here, we estimated a minimum field-level irrigation requirement (I_0 in mm), which can be taken as a conservatively low estimate of irrigation that represents highly efficient irrigation practices.

We used global mapping by crop type to estimate I_0 using a plausible range of published assumptions about water storage capacity. It was assumed that irrigation is just sufficient to replenish lost water without any direct drainage or runoff losses; that is, losses only occur when precipitation exceeds available storage capacity. Following Siebert and Döll (2010), we estimate the available root zone storage (S_{max} in mm) capacity for i=1..26 irrigated crop types based on the estimated harvested area (A_i in ha) of each as contained in the MIRCA2000 dataset (Portmann et al., 2010). These numbers are combined with assumed rooting depth (z_i) and the allowable fraction of depletion of available soil water p_i (Allen et al., 1998) for each crop type as proposed by Siebert and Döll (2010). The plant available water content (θ_a) was estimated using global soil property data (Shangguan et al., 2014; see Appendix A), calculated as the difference between θ at field capacity and permanent wilting point, assumed to correspond to water potential values of -3.3 and -150 m, respectively. In formula:

$$S_{max} = \frac{\sum A_i z_i p_i}{\sum A_i} \theta_a f_{irr} \quad (3)$$

where f_{irr} is the fraction of the grid cell area that is equipped for irrigation (Portmann et al., 2010). This method produced a global average root zone storage of 51 mm per unit of irrigated land, with 90% of values between 10–85 mm, with values depending primarily on the value of z_i.

Because we have observation-based estimates of evaporation, we do not simulate the influence of soil water status on evaporation, but instead, propagate a simple water balance model forced with evaporation estimates. In words, the change in soil moisture storage from one day (S_t) to the next (S_{t+1}) is the net result of gross rainfall onto the irrigated area (P_{irr}), evaporation from the irrigated area (E_{irr}), the minimum irrigation water application required (I_0) and drainage (D), with storage and cumulative fluxes (all in mm):

$$S_{t+1} = S_t + P_{irr} - E_{irr} + I_0 - D \tag{4a}$$

Partial rainfall (P_{irr}) is proportional to the irrigation fraction:

$$P_{irr} = f_{irr}P \tag{4b}$$

It is assumed that any increase in the estimate of evaporation (E'–E) from data assimilation is due to irrigation, where this occurs, and therefore E_{irr} is given by:

$$E_{irr} = f_{irr}E + (E' - E) \tag{4c}$$

Any soil water additions more than maximum storage capacity (S_{max}) are assumed to become drainage, and irrigation is assumed to be just enough to prevent S<0:

$$I_0 = max(E_t - P_g - S_t, 0) \tag{4d}$$

$$D = max(S_t + P_g - E_t - S_{max}, 0) \tag{4e}$$

Rainfall interception losses are included in E. Surface runoff and residual drainage are assumed negligible when $S<S_{max}$. This is an important simplification, but consistent with the definition of a minimum irrigation requirement estimate that reflects optimal efficiency. The daily water balance model was evaluated with an initial state of $S=S_{max}$ and propagated from 2000−2014. The first year was not used in subsequent calculations to allow for artefacts from the initial state chosen.

Evaluation of basin water balance

One test of the accuracy of secondary evaporation estimates is to evaluate whether their inclusion in the basin water balance improves agreement with observations. The difference between E' derived from data assimilation and the background estimate E is interpreted to be derived from lateral inflows:

$$E_{lat} = E' - E \tag{5a}$$

For any basin, the total net amount of discharge from the basin (Q_n) is the result of the gross amount of streamflow generated in all tributaries (Q_g) minus secondary evaporation of flows downstream (E_{lat}) and the change in storage derived from those flows (ΔS_{lat}):

$$Q_n = Q_g - E_{lat} - \Delta S_{lat} \tag{5b}$$

Natural storage variations in soil and groundwater and river channel storage are explicitly simulated by the model and not included in ΔS_{lat}. Storage changes in other surface water bodies (e.g., lakes and reservoirs), river-groundwater exchanges, and induced soil or groundwater storage changes directly related to inundation or irrigation (including pumping) would affect ΔS_{lat}. It is assumed here that the

Hydrol. Earth Syst. Sci. Discuss., https://doi.org/10.5194/hess-2017-757
Manuscript under review for journal Hydrol. Earth Syst. Sci.
Discussion started: 24 January 2018

magnitude of ΔS_{lat} is negligible compared to the other terms if fluxes are averaged over the period 2001–2014. This needs to be considered when interpreting results for individual basins.

We used discharge data for large basins to evaluate whether our estimates of E_{lat} improved the overall agreement between modelled and observed Q_n. The river discharge data used were drawn from the global database of end-of-river discharge records compiled by Dai et al. (2009). This includes data for 925 rivers worldwide. Out of these, we considered only basins for which more than five years of data were available during 1995–2014. This longer period was adopted because few basins had sufficient measurements after 2000. To avoid errors arising from differences in the delineation of basins, we rejected basins with a catchment area less than 100,000 km^2 and those with a reported drainage area that was more than 25% different from the DEM-derived basin area at the river mouth. For the remaining 38 large basins, the temporal and area-average discharge was calculated and compared to the modelled Q_n and Q_g (all in mm y^{-1}).

Closed or endorheic basins represent a special case where Q_n=0 and can also be used to construct a water balance. The 0.05° flow direction grid was used to delineate all internally draining basins located between 72°N and 60°S (further poleward the DEM is affected by land ice). Adjoining endorheic basins were merged into contiguous regions to avoid incorrect basin delineation. From the resulting regions, all those with a surface area greater than 50,000 km^2 were extracted, resulting in 13 contiguous regions. For these regions, Eq. (5b) was evaluated and compared to the expected Q_n=0.

The LST data assimilation changes evaporation without adjusting other water balance terms and hence does not conserve mass balance. In both open and closed basins, this can produce a positive or negative Q_n from Eq. (5b). A difference between estimated and observed Q_n can occur for any of four reasons: Q_g is underestimated, E_{lat} overestimated, ΔS_{lat} is non-negligible, or (for discharging basins only) recorded Q_n is in error.

Evaluation of apparent irrigation water use

Evaluating estimates of secondary evaporation due to irrigation is challenging. Direct observations of evaporation from irrigated land are not widely available, represent point observations, and include primary evaporation. At basin or country level, estimates of irrigation water use can be categorised as ‘bottom-up’ or ’top-down’ estimates. Bottom-up estimates require scaling of estimated crop water use to field-level irrigation requirements. Top-down estimates involve estimating large-scale withdrawals (e.g., by differencing of discharge measurements along a river reach or measured bulk diversions) and accounting for “project” or scheme losses along the distribution network (Bos and Nugteren, 1990). Both approaches have large uncertainties but provide estimates of the order of magnitude of irrigation water use.

Bottom-up estimates of irrigation water use at the global scale and for individual countries are available from previous studies (Siebert et al., 2010; Wada et al., 2014; Siebert and Döll, 2010). They involve soil-vegetation water balance modelling. Similar to the approach used here, these methods require assumptions about root zone storage capacity, the rate of drainage of water from the root zone, the permissible range of root zone soil moisture, and the efficiency of irrigation. Unlike the approach used here, they furthermore require assumptions about evaporation, usually following FAO's crop factor approach (Allen et al., 1998) to model crop water use. The resulting one-dimensional irrigation water requirement estimates are subsequently extrapolated spatially using mapping of areas equipped for irrigation (e.g., Portmann et al., 2010), using assumptions about the number of crop rotations and the area factually irrigated. Each of these assumptions introduces errors and uncertainties. Nonetheless, a comparison with these studies should provide insight into the method developed here.

An important source of uncertainty in our estimation of large-scale I_0 is due to the diffuse spatial distribution of irrigated areas, which is further amplified in current mapping products. The mapping of areas equipped for irrigation contained in the MIRCA2000 dataset (Portmann et al., 2010) was done at 0.08° grid resolution and linearly interpolated to 0.05° resolution in this study. Even at this high resolution, a large proportion of total irrigable land occupies only a small fraction of a grid cell (Figure 2).

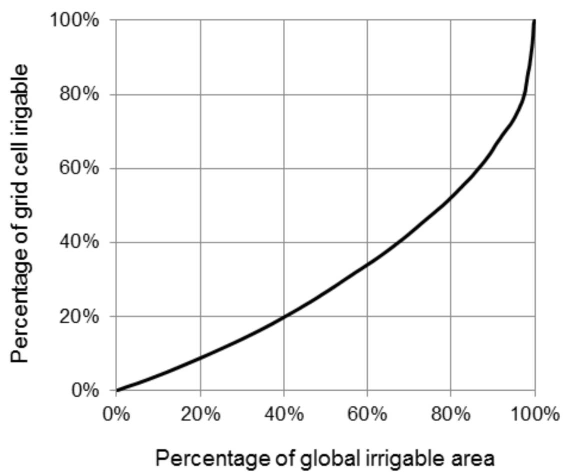

Figure 2. Cumulative distribution curve or quantile plot describing the degree to which the global irrigable area is concentrated. It shows that, at 0.05° grid resolution, almost half of the total global irrigable area occupies less than 25% of a grid cell.

The degree of concentration differs between countries for two reasons. Firstly, the true distribution of irrigation land varies; for example, irrigation tends to be highly concentrated in large surface water irrigation schemes (e.g., the Nile delta and Indus floodplains) but can be highly distributed where supplementary irrigation water is drawn from unregulated streams or groundwater. Secondly, the quality, resolution and predictive value of information related to irrigation area varies widely, which affects the accuracy of mapping (Portmann et al., 2010). The distribution of irrigation land introduces uncertainty in the attribution of E' in grid cells with small fractions of irrigated land. We expect that the fraction of a grid cell that needs to be irrigated to create a measurable LST signal may be around 10% but will vary spatially depending on the LST contrast between irrigated and non-irrigated land. To account for this uncertainty, we calculated the mean I_0 (Eq. 4) per unit irrigation area for all grid cells with more than, respectively, 1, 2, 5, 10 and 25% of the area equipped for irrigation. These estimates were subsequently multiplied with the total area equipped for irrigation in each country. The coefficient of variation among the five estimates was calculated as a measure of estimation uncertainty.

The AQUASTAT database (FAO, 2017) provides country-level estimates of agricultural water withdrawal (W in km^3 y^{-1}) from surface and groundwater. The estimates are derived by different methods for different countries, and likely include both bottom-up and top-down techniques. Estimates also relate to different periods or years. Despite these uncertainties, they currently represent official international statistics for each country. Any comparison of field-level irrigation water application (I_0) and large-scale water withdrawal (W) needs to account for inefficiencies in the entire water distribution network. These include evaporation, leakage and return flow on- and off-farm. 'Project efficiencies' that express the ratio of I_0 over W can be estimated in principle, but this requires detailed ancillary data (Bos and Nugteren, 1990). In their global modelling study, Siebert and Döll (2010) proposed ratios range from 0.25 for irrigation dominated by paddy rice to 0.70 for efficient crop irrigation methods in Canada, Northern Africa and Oceania. We did not assume values but instead calculated an 'apparent' bulk project efficiency for each country, by dividing the ratio of modelled I_0 over W reported in AQUASTAT. The credibility of the resulting values was subsequently interpreted within the framework developed by Bos and Nugteren (1990).

Secondary evaporation and the global water cycle

Total secondary evaporation was estimated as the sum of open water evaporation plus the difference $E'-E$, representing the difference between modelled primary evaporation E for a situation where precipitation is the only source of water (the background estimate) and total evaporation E' resulting from LST assimilation (the analysis estimate). The resulting estimate of total secondary evaporation is a hypothetical and model-based quantity. Evaporation in the absence of lateral flows is counterfactual and not necessarily accurately estimated by the model, particularly in humid environments. Furthermore, all open water evaporation was included in secondary evaporation; we did not attempt to estimate the evaporation that might have occurred from the surface had it not been covered by water.

The difference $E'-E$ was distributed dynamically in proportion to the magnitude of each of three evaporation terms (i.e., transpiration, soil evaporation, and open water evaporation; wet canopy evaporation was left unchanged). A component of secondary evaporation was attributed to irrigation following the method described earlier. The remainder could be attributed to permanent water bodies,

Hydrol. Earth Syst. Sci. Discuss., https://doi.org/10.5194/hess-2017-757
Manuscript under review for journal Hydrol. Earth Syst. Sci.
Discussion started: 24 January 2018

ephemeral water bodies, and a residual component that includes any evaporation from replenished wetlands and floodplains, as well as any use of groundwater sources beyond that simulated by the model to occur from shallow groundwater (Peeters et al., 2013).

Results

Basin water balance

The combined surface area of the 51 basins used in evaluation (38 ocean-draining and 13 closed basins) was 63 million km^2 or 47% of the ice-free land surface area (Figure 3). For each region, the period-average measured discharge (zero in the case of closed basins) was compared with modelled Q_g and Q_n (Figure 4, Table 1). Overall, accounting for secondary evaporation produced a very small improvement in the correlation between observed and estimated discharge (Figure 4ab). However, the largest error contribution was from basins with high discharge rates, where secondary evaporation represents a small fraction of Q_g. A clearer improvement in the agreement was found for basins with less than 300 mm y^{-1} net discharge (Figure 4cd). The explained variance (R^2) increased from 0.67 to 0.71, and there was a reduction of the bias from +38 to +2 mm y^{-1}. Water balance estimates were improved considerably for several basins, including the Indus River ('I' in Figure 4cd), Nile River, the Great Basin in the USA, and the African Rift Valley (Table 1). The agreement could not improve where Q_g estimates were already lower than observed, such as the Paraná and Fitzroy Rivers ('P' and 'F' in Figure 4cd). Water balance estimates for some closed basins were also degraded, evident from negative Q_n values (e.g., the South Interior and Rukwa basins in Southern Africa), implying that Q_g was underestimated, secondary evaporation overestimated, or both (Table 1).

Hydrol. Earth Syst. Sci. Discuss., https://doi.org/10.5194/hess-2017-757
Manuscript under review for journal Hydrol. Earth Syst. Sci.
Discussion started: 24 January 2018

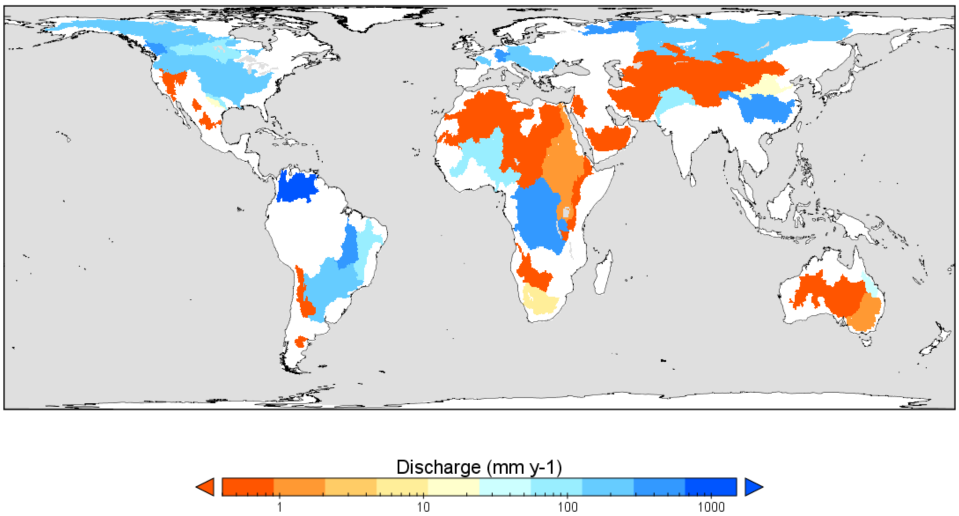

Figure 3. Extent and area-average annual discharge for the 38 ocean-draining (orange to blue) and 13 closed basins (dark orange) used in the evaluation. The two darkest blue colours indicate a discharge in excess of 300 mm y^{-1}.

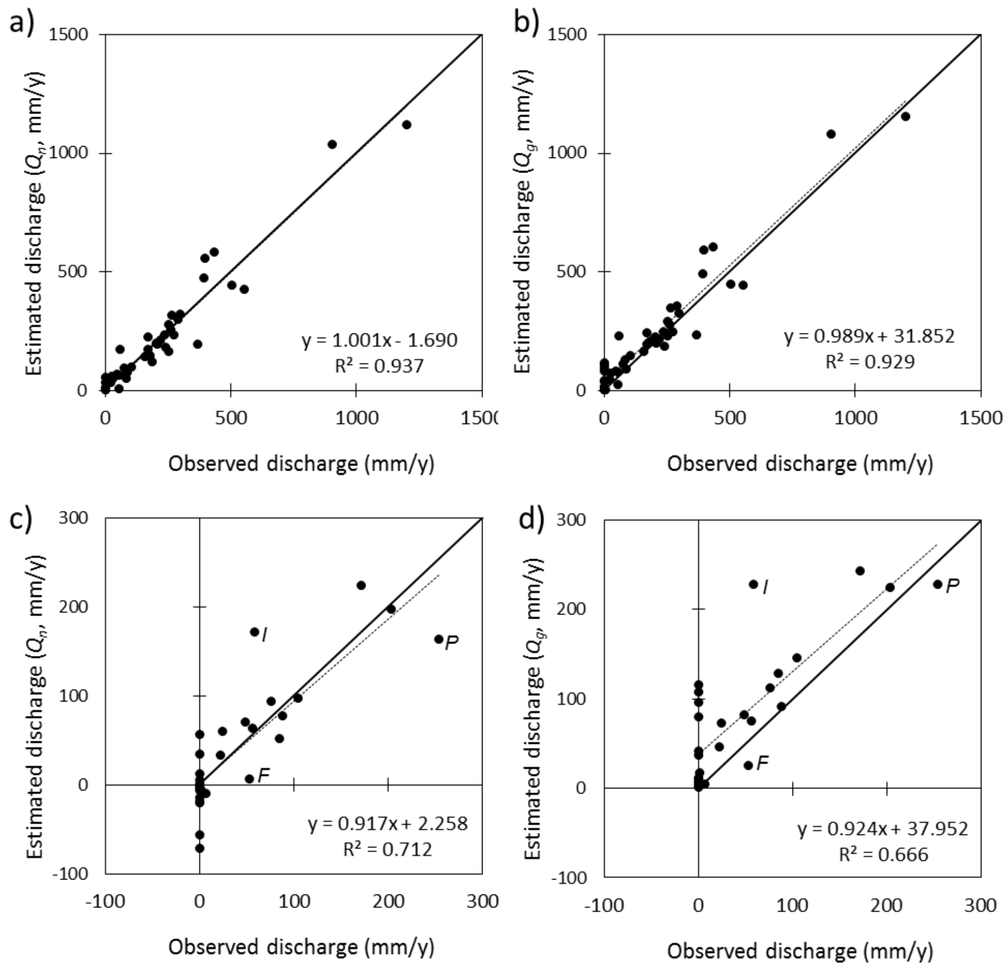

Figure 4. Comparison of observed basin-average discharge (mm y^{-1}) for large basins that are internally draining (i.e., zero discharge) or have adequate station discharge data with model estimates of (a) net discharge (Q_n), that is, gross discharge (Q_g) minus secondary evaporation, and (b) Q_g only. (c) and (d) data for discharge below 300 mm y^{-1} only (cf. Table 1). Letters indicate Indus (I), Paraná (P), and Fitzroy (F) River.

Table 1. Area-average discharge (mm y^{-1}) for selected basins as observed and estimated by the model in the presence (Q_n) and absence (Q_g) of secondary evaporation, respectively. Listed data for basins with discharge less than 300 mm y^{-1} only (cf. Figure 4cd).

Area-average basin discharge (mm y^{-1})		estimated	
	Observed	Q_n	Q_g
Closed river basins			
Great Basin, US	-	1	42
Guzman, North America	-	-6	3
Mairan-Viesca, Mexico	-	-15	7
Patagonia, South America	-	5	10
Titicaca-Chiquita, South America	-	-19	38
North Interior, Africa	-	-4	4
South Interior, Africa	-	-71	12
Rukwa, Africa	-	-56	115
Rift Valley, Africa	-	35	107
Jordan	-	-1	8
Arabian peninsula	-	0	1
Central Asia	-	57	80
Central Australia	-	-20	8
Ocean-reaching rivers			
Nile, Africa	0	13	96
Murray, Australia	1	-5	17
Orange/Senqu, Africa	7	-9	4
Colorado, US	23	33	46
Huanghe, China	24	61	73
Burdekin, Australia	48	70	82
Parnaiba, Brazil	76	94	113
Brazos, US	57	64	76
Fitzroy, Australia	54	6	26
Indus, Asia	58	172	228
Sao Francisco, Brazil	105	97	146
Niger/Issa Ber, Africa	88	78	92
Nelson, Canada	85	52	129
Paraná, South America	255	163	228
Elbe/Labe, Europe	172	224	243
Mississippi, US	204	198	225

Irrigation water requirements

Spatiotemporal estimates of I_0 at 0.05° and daily time step were aggregated to country-level estimates in km^3 y^{-1} (Table 2). Also calculated were the coefficient of variation in I_0 estimates (CV_{I0}) caused by the treatment of 'mixed pixels' in irrigation mapping, FAO-reported annual *W*, and the apparent project irrigation efficiency. Global I_0 for 2001–2014 was 680 km^3 y^{-1} (standard deviation 110 km^3 y^{-1}). This value is lower than estimates of contemporary irrigation water use reported in the literature of 1092 km^3 y^{-1} (Döll and Siebert, 2002), 1180 km^3 y^{-1} (Siebert and Döll, 2010) and 994–1179 km^3 y^{-1} (Wada et al., 2014). Estimates of I_0 listed for seven countries by Döll and Siebert (2002) were all higher than those found here (Table 2), and even more than double for the USA (112 vs. 48 km^3 y^{-1}) and Spain (21 vs 5.1 km^3 y^{-1}). Quoted independent estimates were 113 km^3 y^{-1} for the USA (Solley et al., 1998) and 15 km^3 y^{-1} for Spain (J.A. Ortiz cited in Döll and Siebert, 2002).

Table 2. Irrigation water withdrawal (*W*) as reported to FAO for the 20 countries with largest agricultural withdrawals, along with the estimated minimum field-level irrigation requirement (I_0), the coefficient of variation in I_0 estimates (CV_{I0}) and the apparent project efficiency (I_0 / *W*).

Country	*W*	I_0	CV_{I0}	I_0 / *W*
	km^3 y^{-1}	km^3 y^{-1}	-	-
India	688	152	0.07	0.22
China	392	105	0.13	0.27
United States of America	175	48	0.20	0.27
Pakistan	172	49	0.01	0.28
Indonesia	93	14	0.10	0.15
Iran	86	5	0.22	0.06
Viet Nam	78	15	0.05	0.19
Philippines	67	5	0.16	0.07
Egypt	67	30	0.02	0.44
Mexico	62	19	0.22	0.31
Japan	54	4	0.23	0.07
Iraq	52	5	0.19	0.10
Thailand	52	16	0.09	0.32
Uzbekistan	50	11	0.02	0.21
Brazil	45	16	0.39	0.36
Turkey	34	6	0.36	0.16
Bangladesh	32	20	0.08	0.63
Burma	30	13	0.21	0.43
Chile	29	2	0.22	0.07
Argentina	28	5	0.47	0.17
Global	**2,767**	**680**	**0.16**	**0.25**

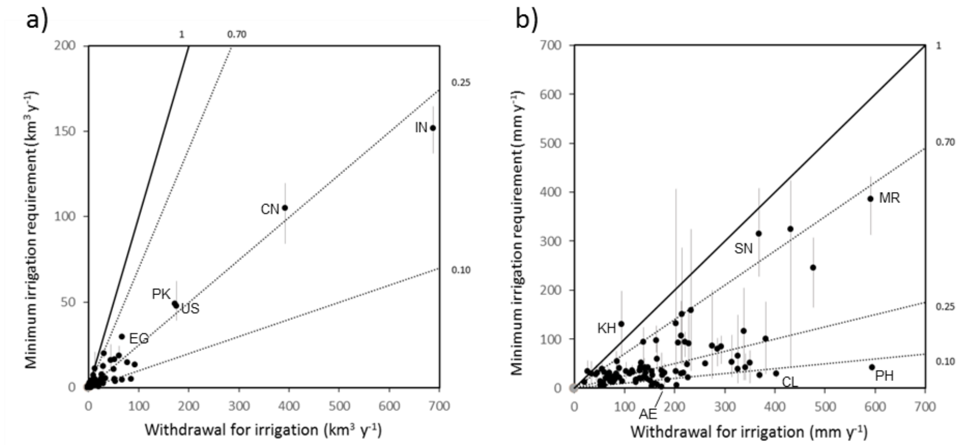

Figure 5. Comparison of country-level agricultural water withdrawal (W) (FAO, 2017) and estimated minimum irrigation requirement (I_0) expressed as (a) total volume, and (b) depth per unit area of area equipped for irrigation for countries with >1 km^3 y^{-1} withdrawals (N=91). Dotted lines show apparent project efficiencies between the two quantities. Countries indicated are (in a) Egypt (EG), Pakistan (PK), United States (US), China (CN) and India (IN), and (in b) Cambodia (KH), Senegal (SN), Mauritania (MR), United Arab Emirates (AE), Chile (CL), and the Philippines (PH).

The I_0 explains 96% in the variance in W by country (Figure 5a), but total variance is dominated by only four countries, and the area equipped for irrigation explains already explains 86% of the variance. Volumes were divided by the total area equipped for irrigation to normalise for these effects. Normalised I_0 explained 38% of the variance in normalised W (Figure 5b). A high correlation between the two is not necessarily to be expected, as country-average project efficiencies will vary (represented by the lines in Figure 5b). For example, a low efficiency is inferred and would be expected in the Philippines, where irrigation is dominated by paddy rice agriculture, whereas higher efficiencies would be expected in large schemes in arid countries such as Egypt and Mauritania. Nonetheless, apparent efficiencies are generally lower than would be expected based on benchmark estimates provided by Bos and Nugteren (1990). For example, using global volumes of I_0 and W, a project efficiency of 0.25 is calculated. This is lower than estimates of 0.36–0.43 assumed in previous studies (Döll and Siebert, 2002; Wada et al., 2014; Siebert and Döll, 2010). Physically impossible or implausible project efficiencies were also calculated for some countries, including Cambodia (I_0/W >1), and the United Arab Emirates and Chile (I_0/W<0.1) (Figure 5b). Possible explanations for this will be discussed.

Secondary evaporation and the global water cycle

We estimate that secondary evaporation contributed 41.2 mm y^{-1} or 8.1% to total evaporation from the global land area during 2001−2014 (Table 3), equivalent to 5.4% of terrestrial precipitation (759 mm y^{-1}) and 16% of generated streamflow (258 mm y^{-1}). Globally, only a very small percentage of all secondary evaporation (5%) was due to irrigation. Overall more important pathways for secondary evaporation were evaporation from permanent water bodies (48%), enhanced transpiration associated with wetland vegetation or greater-than-predicted groundwater uptake (27%), enhanced soil evaporation (11%), and evaporation from ephemeral water bodies (10%). Surface and groundwater inputs enhance global plant transpiration by an estimated 12.1 mm y^{-1}, representing a 4.4% increase. Of this increase, 10% can be attributed to irrigation.

Table 3. Estimates of annual primary and secondary evaporation (E in mm y^{-1}) components for 2001−2014 expressed as water depths across the global terrestrial area ($149\cdot10^6$ km^2).

	Primary E	Secondary E	*Total*	Irrigation only
wet canopy E	81.3	–	***81.3***	–
transpiration	278.7	12.1	***290.8***	1.2
soil E	107.0	4.9	***111.9***	0.5
E from ephemeral water	–	4.6	***4.6***	0.3
E from permanent water	–	19.6	***19.6***	–
Total	***467.0***	***41.2***	***508.2***	***2.0***

The spatial distribution of evaporation from irrigation areas (Figure 6a) and permanent water bodies (Figure 6b) largely reflects the irrigation and water mapping input data, respectively. The spatial distribution of other sources of secondary evaporation provides some new insights (Figure 6c). Globally, some areas with the greatest secondary evaporation volumes include receiving floodplains in tropical monsoonal regions. The main regions in South America include the Gran Chaco and Pantanal plains and Amazon floodplains (Figure 7). The main regions in Africa the Southern Interior basin in Botswana and surrounding countries (including the Okavango Delta and other wetlands), and the floodplains of the White Nile River in South Sudan and the Inner Niger Delta (Figure 8). Other areas with high secondary evaporation rates include the Yucatan peninsula in Mexico (Figure 7), the boreal wetlands and ephemeral lakes of Canada and Scandinavia (Figure 7 and Figure 8, respectively), and the salt lakes and floodplains of inland Australia (Figure 9).

Hydrology and Earth System Sciences
Open Access
Discussions

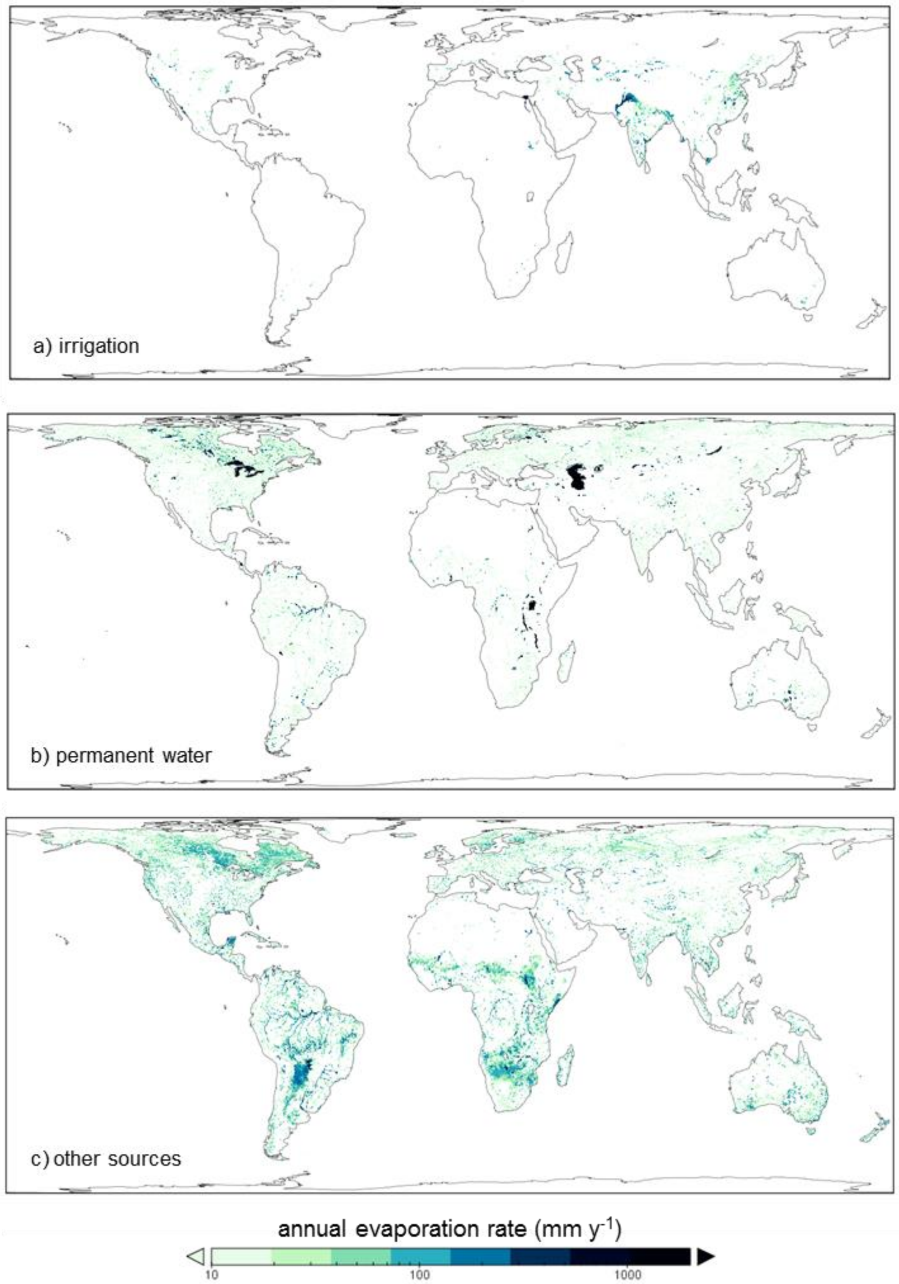

Figure 6. Spatial distribution of estimated secondary evaporation losses derived from (a) irrigation, (b) permanent water bodies, and (c) other sources, including wetlands and floodplains.

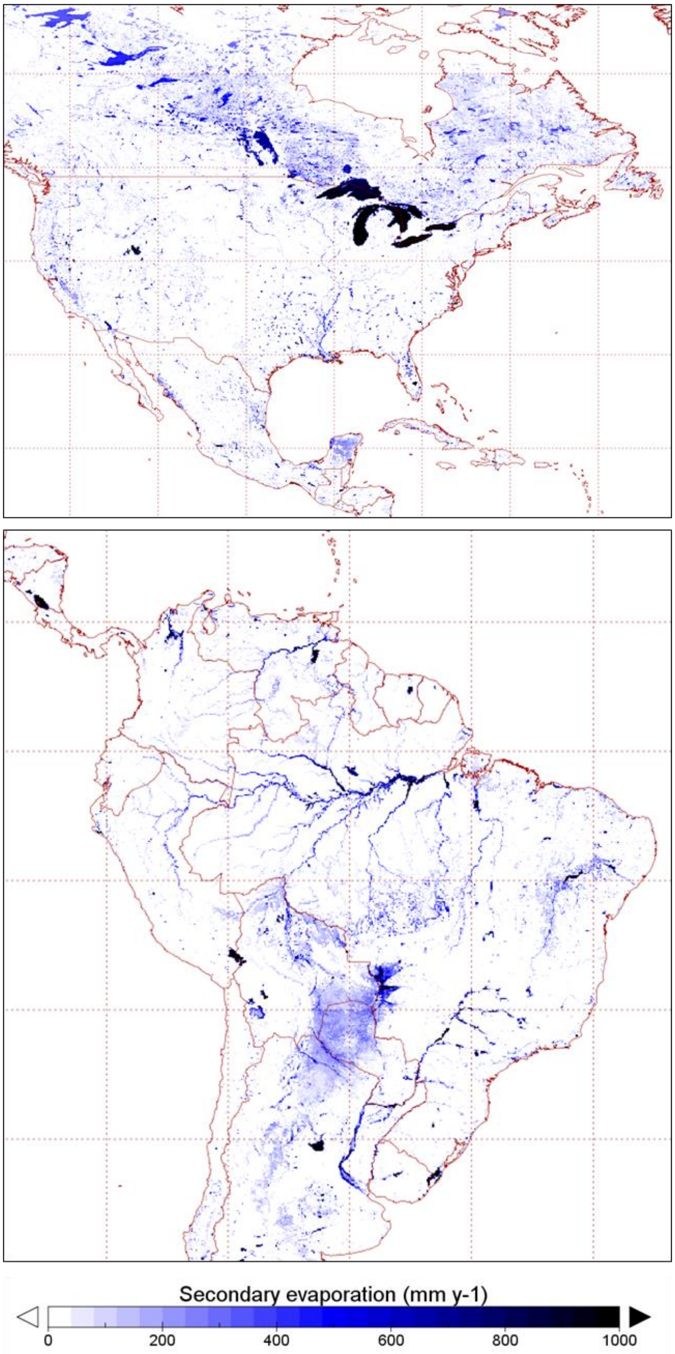

Figure 7. Spatial distribution of secondary evaporation losses in the Americas.

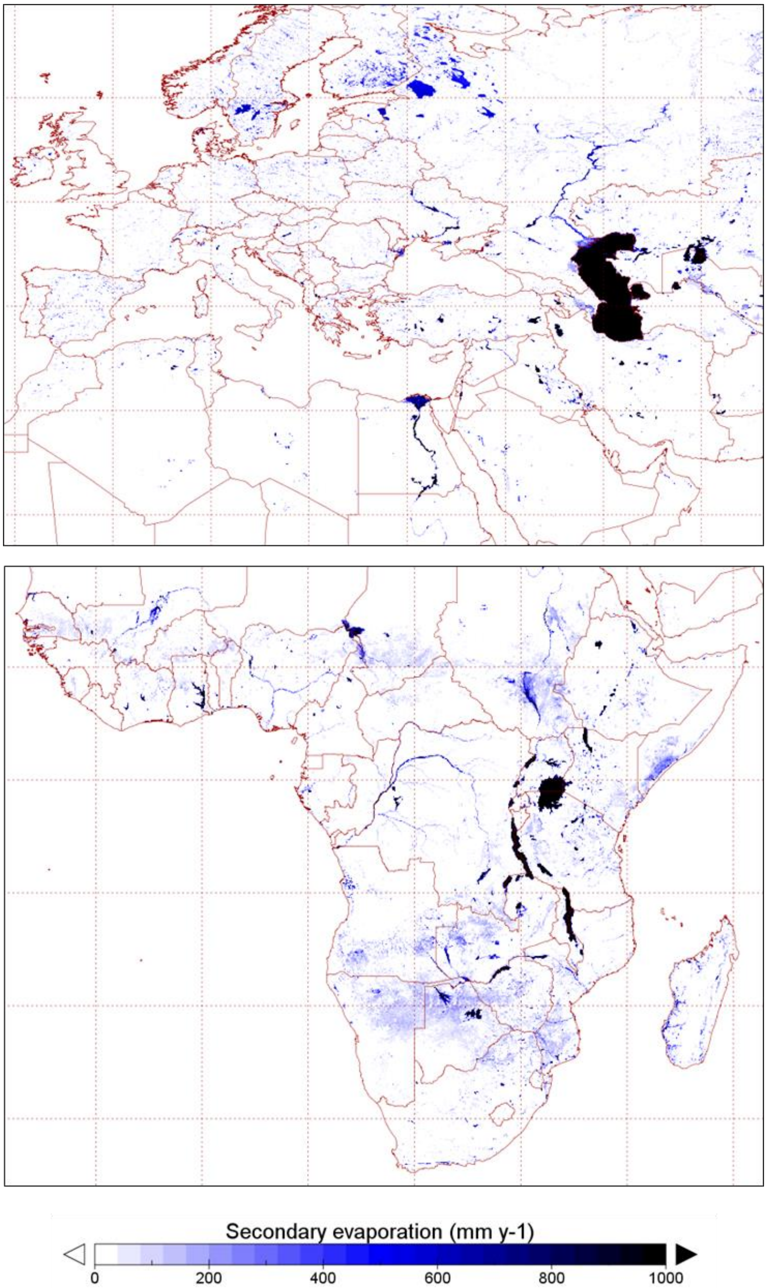

484 Figure 8. Spatial distribution of secondary evaporation losses in Eurasia and Africa.

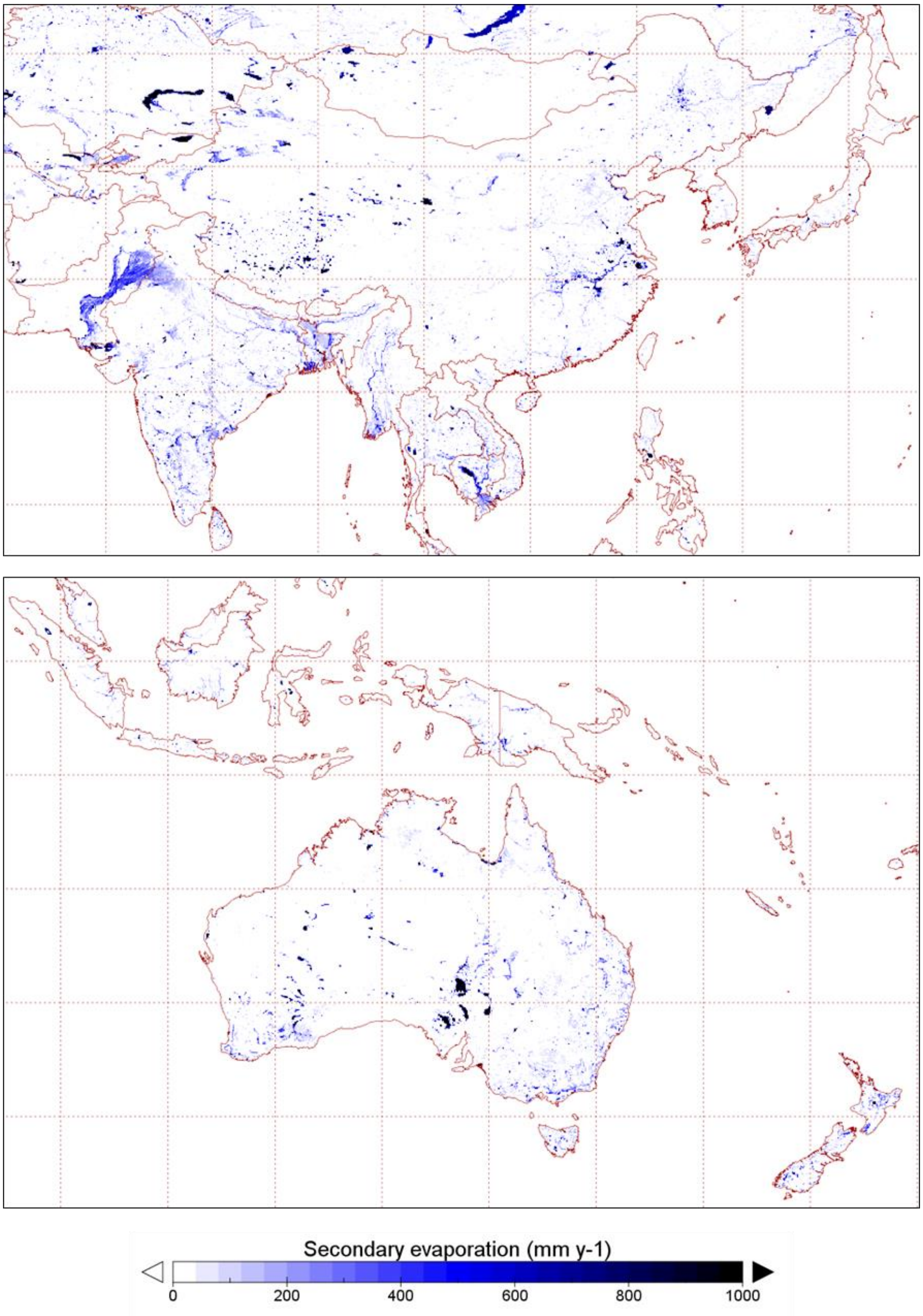

486

487 Figure 9. Spatial distribution of secondary evaporation losses in Eastern Asia and Oceania.

488

Hydrol. Earth Syst. Sci. Discuss., https://doi.org/10.5194/hess-2017-757
Manuscript under review for journal Hydrol. Earth Syst. Sci.
Discussion started: 24 January 2018

Hydrology and Earth System Sciences
Open Access
Discussions

Discussion

Uncertainties in evaporation estimation

The uncertainty in estimates of secondary evaporation arises from three main sources: (1) estimation of 'background' evaporation E; (2) estimation of surface water evaporation; and (3) estimation of total evaporation E' by LST assimilation. A formal assessment of error in each of these terms is not possible for lack of observations and will vary in space and time. Below we discuss what we expect to be the main sources of uncertainty in each component.

An error in background model E may be compensated by data assimilation, but still leads to an error in the estimated secondary evaporation, calculated as E'–E. The main sources of error in E vary as a function of environmental conditions and the quality of the measurement network. In water-limited environments, the most likely sources of error in E are errors in precipitation estimates and the simulation of water availability in the root zone. The quality of precipitation estimates is relatively poor in many of the world's dry regions (Beck et al., 2017). Information on the ability of vegetation to access deeper soil moisture and groundwater is important, particularly in ephemerally wet systems, but is not available at the global scale. In humid environments, the most likely sources of error in E are in the estimation of rainfall interception losses, the net available energy for evaporation, and surface conductance. As part of earlier model development, background E was compared with estimates derived from flux tower observations and compared with alternative ET estimation methods (Yebra et al., 2013; Van Dijk, unpublished). These evaluations showed little if any systematic bias and a standard difference of 135–168 mm y^{-1} across sites (N=16–168). This total difference also includes errors in the flux tower-derived estimates and differences arising because the tower footprint is not representative of the grid cell. Therefore the true error in our estimates will be lower.

Observation-based estimates of large-area evaporation from water bodies, wetlands and irrigated areas (i.e. >0.05°) are scarce. Some site measurements of wetland and irrigation evaporation have been published (e.g., Guerschman et al., 2009) but typically reflect an environment with very high spatial variation and therefore often cannot easily be compared to estimates at 0.05°. A coordinated effort that collates observations of secondary evaporation and combines these with historical time series remote sensing imagery (cf. Figure 1a) to generate estimates at a more representative spatial scale would appear necessary and valuable.

Errors in the estimation of surface water evaporation are the combined result of errors in the estimation of open water evaporation rate and the mapping of surface water extent. Open water evaporation rate was estimated using the Priestley and Taylor (1972) approach. An important uncertainty in this approach is that it does not account for strong contrasts in near-surface water temperature. Surface water extent was mapped using 8-day MODIS shortwave infrared (SWIR) reflectance composites (Van Dijk et al., 2016). Systematic overestimation of water extent can occur in low relief regions with very low SWIR reflectance (e.g., lava outflows), whereas underestimation can occur in regions with a dense elevated canopy that prevents water detection (e.g., floodplain forests or mature flooded crops).

The LST assimilation mitigates estimation errors in background and open water evaporation but is also subject to uncertainties of its own. The technique developed here relies on the assumption that there is a perfect correlation between spatial LST anomalies at the time-of-overpass (around 10 am local time) and daytime (sunrise-sunset) average values, or at least for the low-relief areas where LST was assimilated. In reality, there can be spatial differences in the temporal rate of LST change, for example as a function of spatial differences in heat storage capacity and aerodynamic conductance (Kalma et al., 2008). Furthermore, we assumed a constant, maximum bias-adjusted error of 1K in the difference between observed and model background LST. Each of these choices can have affected the efficacy of the assimilation.

Nonetheless, assessment of temporal patterns in E' (such as in Figure 1e) and the spatial patterns in secondary evaporation (Figures 6–9) agree with known areas receiving lateral inflows (e.g., wetlands) or irrigation. Less expected were the widespread high secondary evaporation rates in the northern Yucatan peninsula in Mexico and the Southern Interior in Southern Africa. The northern Yucatan peninsula is a low lying region with karst geology and forest are known to access shallow groundwater (Bauer-Gottwein et al., 2011). The Southern Interior includes several terminal wetlands (e.g., the Okavango Delta) and has unconsolidated alluvial deposits that contain productive aquifers (MacDonald et al., 2012) and it is plausible that at least some of the vegetation has access to deeper soil moisture or groundwater. In both cases, the background evaporation estimate (E) is constrained by precipitation and the corresponding simulated presence of soil- and groundwater within the root zone (E). Any underestimation of E leads to an increased estimate $E'–E$ and therefore an increased estimate of secondary evaporation, without necessarily implying that all the water involved is derived from later inflows. An alternative measure of the importance of secondary evaporation is $E'–P$ (Figure 10). These results suggest that period-average E' exceeds P by in the order of 100 to 200 mm y^{-1}. For the Southern Interior basin, we found an apparent overestimation of c. 72 mm y^{-1} (Table 1) which suggests that at least some of this difference is realistic. Underestimation of precipitation may also go some way towards explaining these differences: both regions are in transitional climates with a relatively strong, non-orographic precipitation gradient of 900–1400 mm y^{-1} (Yucatan) and 400–1100 mm y^{-1} (Southern Interior), respectively. Combined with a low density of rainfall gauges (Hijmans et al., 2005), these gradients make a systematic bias in rainfall estimates more plausible.

Hydrol. Earth Syst. Sci. Discuss., https://doi.org/10.5194/hess-2017-757
Manuscript under review for journal Hydrol. Earth Syst. Sci.
Discussion started: 24 January 2018

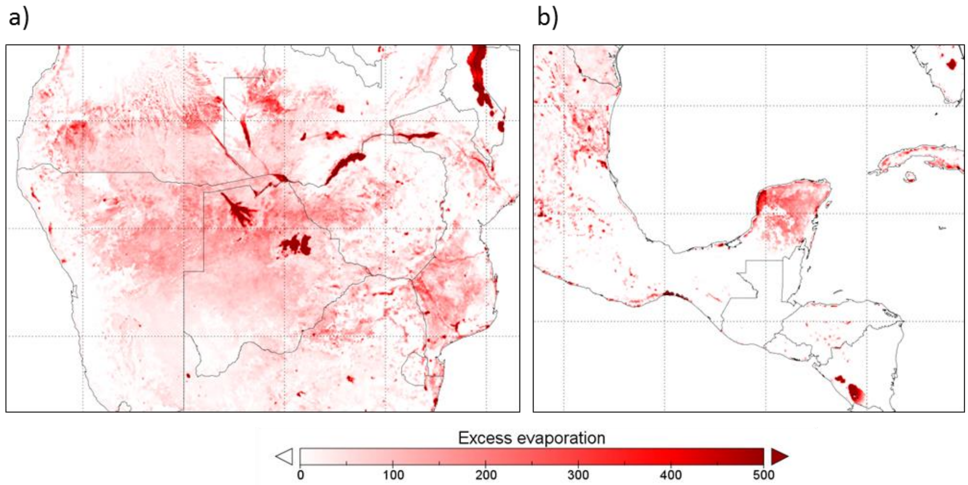

Figure 10. Mean difference between total evaporation and precipitation for 2001–2014 for (a) Botswana and (b) the Yucatan peninsula, and surrounding areas.

Uncertainty in irrigation water requirement estimation

The total estimate of minimum irrigation water requirement (I_0) at the global scale was about a third lower than previous model-based estimates (Siebert et al., 2010; Wada et al., 2014; Siebert and Döll, 2010). There are some likely explanations for this. Firstly, the diffuse distribution of areas equipped for irrigation (Figure 2) means that the LST signal from irrigation will likely have been too small to estimate the associated I_0 correctly everywhere. An insufficient LST signal is most likely for grid cells and countries with a temperate and humid climate and highly distributed irrigation, such as the US, where our estimate of I_0 was twice smaller than published previously. Conversely, irrigation evaporation estimates should be more accurate in hot, arid regions with large and concentrated irrigation, such as Egypt's Nile Delta (Figure 1). The temporal pattern of the evaporative fraction for this grid cell corresponds well with that of vegetation cover (Figure 1e) and assumes values that appear realistic, even more so when considering that only around 80% of the grid cell was irrigated (Figure 1a).

Second, previous studies have estimated crop water use (and from that, I_0) using the FAO method of Allen et al. (1998). This method assumes a well-growing crop not affected by ineffective or insufficient irrigation, unfavourable weather, nutrition or soil, pests and diseases, or other growth-limiting factors. The resulting crop water use estimates are likely to represent idealised conditions and may be higher than actual water use.

Third, errors in irrigation area mapping are also likely to have played a role. It is noteworthy that the MIRCA2000 mapping used here (Portmann et al., 2010) indicated that 100% of the grid cell in Figure

1a was equipped for irrigation. This is not the case: most unirrigated areas are settlements. Previous studies will have assumed the entire area was available for irrigation and this difference alone would cause their I_0 estimates for this particular grid cell to be 25% higher. While these numbers relate to just a single grid cell, it serves to demonstrate that incorrect mapping of irrigation areas can have considerable impact on our I_0 estimates. As another example, any irrigation outside the grid cells indicated to have at least some irrigable area in the MIRCA2000 mapping would be wholly attributed to non-irrigation forms of secondary evaporation.

Despite these caveats, it is highly likely that true irrigation water application is greater than our estimate I_0, as it was defined as a hypothetical quantity that might occur under conditions of optimally efficient irrigation. Previous studies have made similar assumptions. In reality, field-level irrigation efficiency is reduced by additional drainage below the root zone and any surface runoff that may occur. Further uncertainties are introduced through the necessary assumptions about rooting depth and root zone storage capacity. The comparison with FAO-reported W estimates suggests project efficiencies that are lower than those assumed in previous studies, but the overall correlation between country I_0 and W volumes was high, and could not solely be attributed to differences in irrigated area (Figure 5). A comparison of country I_0 and W expressed as area-average rates indicates contrasts in project efficiency that are expected in several cases. In other cases, values are outside a plausible range. At least some of these poor estimates are likely related to the mentioned inaccuracies in irrigation mapping (e.g., Chile and the United Arab Emirates in Figure 5b).

Overall, the method developed here shows a promising approach to estimate irrigation water use. Estimation at an even higher spatial resolution should help to detect the LST signal more accurately where irrigation areas are dispersed and so produce better estimates of E'. This provides a powerful argument in support of 'hyper-resolution' water balance observation and modelling (Wood et al., 2011). All satellite-derived inputs are available at a resolution that is about an order of magnitude finer (500–1000 m) than used here, and computationally data assimilation at this resolution is also already feasible. The main impediment is the resolution and quality of irrigation area mapping, which is required to attribute secondary evaporation to irrigation and other sources. The E' estimates themselves may assist in mapping, along with information on temporal vegetation patterns, open water mapping and relief, among others. This is an avenue we hope to pursue in future.

Importance of secondary evaporation in the global water cycle

Our analysis suggests that secondary evaporation makes a meaningful contribution to global evaporation (8.1%) and reduces the amount of discharge to the oceans by c. 16%. At the global scale, irrigation is responsible for only a small fraction of this reduction (c. 5%), with the remainder occurring from water bodies and wetlands. These global averages hide significant regional variation. For example, irrigation plays an important role in the evaporation of river flows in the Nile, Indus and Murray-Darling basins, where most of the discharge is evaporated before reaching the ocean. About half of total global secondary evaporation is from permanent freshwater bodies, including from some very large water bodies such as the Caspian Sea, the Great Lakes, and the African Rift Valley Lakes.

We estimated global terrestrial evaporation to be 508 mm y^{-1} per unit land area or $75.5\cdot10^{12}$ m^3 y^{-1} total for 2001–2014, made up of 467 mm y^{-1} or $69.6\cdot10^{12}$ m^3 y^{-1} primary evaporation and 41.2 mm y^{-1} or $6.1\cdot10^{12}$ km^3 y^{-1} secondary evaporation. This is close to estimates derived from previous studies. For example, Miralles et al. (2016) reported 13 estimates of terrestrial E, derived from a variable combination of satellite observations and modelling, with an average value of $69.2\cdot10^{12}$ km^3 y^{-1} and coefficient of variation (CV) of ±10%. Schellekens et al. (2017) reported a mean of $74.5\cdot10^{12}$ km^3 y^{-1} (CV of ±6%) for an ensemble of 10 state-of-the-art global hydrological models and land surface models. Some of these differences are attributable to the differences in total area and period considered, but the different datasets also includes secondary evaporation losses to different degrees. Given these represent 8% of total evaporation, such inconsistencies help to explain differences between estimates.

The partitioning between primary evaporation components is within the range of recently published estimates, though noting that those ranges are broad (Table 4). Secondary evaporation is fully responsible for open water evaporation and has no impact on wet canopy evaporation; both are a logical consequence of the way these terms are conceptualised. It is estimated that global transpiration and soil evaporation are both enhanced by about 4.5% due to secondary evaporation of surface and groundwater resources. Irrigation is responsible for a tenth of this increase, with the remainder due to natural processes. Because of the coupling between transpiration and carbon uptake, it can be assumed that these enhancements will increase global carbon uptake by a similar proportion. Once again these small contributions apply at global scale, but there are strong differences locally and regionally.

Table 4. Estimated percentage of total (or, between brackets, primary) terrestrial evaporation (*E*) contributed by different pathways, compared with estimates from two recent studies.

Percent of total E	this study	Zhang et al. (2016)	Miralles et al. (2016)
wet canopy E	16 (17)	10	10-24
transpiration	57 (60)	65	24-76
soil E	21 (23)	25	14-52
open water E	4 (0)	–	–

Thiery et al. (2017) simulated the global impact of irrigation using coupled land surface and atmosphere models. They estimated an evaporation increase from irrigation of 418 km^3 y^{-1}; of similar magnitude to the 300 km^3 y^{-1} we found. Despite this small contribution to total global evaporation, their modelling did predict small but meaningful reductions in high-temperature extremes over and near large irrigation areas; irrigation rates tend to be highest during hot and dry conditions. To the best of our knowledge, there have been no studies on the impact of wetlands and water bodies on regional and global climate so far. Given that we estimate these other forms of secondary evaporation to be twenty times greater than from irrigation, their impact on the atmosphere should be significant.

Conclusions

We presented a methodology to assimilate thermal satellite observations into a global hydrological model W3 at a resolution of 0.05° to estimate secondary evaporation of surface and groundwater resources. In addition, we used a simple irrigation water balance model to estimate minimum irrigation requirement (I_0) globally. Our main conclusions are as follows.

(1) The method developed produces realistic temporal and spatial patterns in secondary evaporation. Accounting for secondary evaporation measurably improved water balance estimates for large closed and open basins, reducing bias in the overall water balance closure from +38 to +2 mm y^{-1}.

(2) Our I_0 estimates were lower than country-level estimates of irrigation water use produced by other model estimation methods, for three reasons. Firstly, at the 0.05° resolution, much of global irrigated land occupies only a small part of individual grid cells and may not reduce LST sufficiently to be accurately estimated. Second, our I_0 estimates reflect actual evaporation, which can be lower than idealised crop water use estimates used in previous studies. Third, spatial errors in irrigation area mapping directly affect the attribution of secondary evaporation to irrigation. Overall, actual irrigation application will most likely be higher than estimated here but possibly lower than reported previously.

(3) The role of irrigation water use in secondary evaporation is minor at the global scale, accounting for 5% of total secondary evaporation and 0.4% of total terrestrial evaporation. Nonetheless, water withdrawals and irrigation evaporation are an important part of the water balance in some regions.

(4) Around 16% of globally generated water resources evaporate before reaching the oceans, enhancing total terrestrial evaporation by 8.8%. Of this secondary evaporation, 5% is evaporated from irrigation areas, 58% from water bodies, and 37% from other surfaces.

(5) Lateral inflows of surface and water resources were estimated to increase global plant transpiration by c. 4.5%. The impact on global carbon uptake would be expected to be of similar magnitude. Previous studies have predicted that irrigation evaporation affects regional and global climate. Given evaporation from wetlands and permanent water bodies is an order of magnitude larger, their impact on the climate system should be pronounced.

There is scope for further improvement in accounting for natural and anthropogenic secondary losses by applying the model-data assimilation approach developed here at higher resolution. This is conceptually straightforward and computationally achievable. Key developments required include more accurate and detailed dynamic observational data on surface water dynamics and more accurate mapping of areas equipped for irrigation.

Data availability

The 5-km water balance estimates presented here will be available via *http://www.wenfo.org/wald/*.

Acknowledgements

The MODIS products were retrieved from the online Data Pool, courtesy of the NASA EOSDIS Land Processes Distributed Active Archive Center (LP DAAC), USGS/Earth Resources Observation and Science (EROS) Center, Sioux Falls, South Dakota, https://lpdaac.usgs.gov/data_access/data_pool. Albert van Dijk was supported under Australian Research Council's Discovery Projects funding scheme (project DP140103679).

Author contribution

AVD conceptualised the study. JS, HB, AW and GD developed global input data for the modelling. MY developed the remote sensing evaporation scheme. LR assisted in the development of the data assimilation approach. AVD carried out the analysis and wrote the first draft manuscript. All other authors contributed to the analysis, interpretation and writing.

Appendix A. Global data sets used

- *Climate* forcing data used included the MSWEP multi-source merged precipitation product version 1.1 (Beck et al., 2017) and the WFDEI dataset version 1 (Weedon et al., 2014) for other atmospheric variables (short- and longwave down-welling radiation, screen-level air temperature and humidity, wind speed, snowfall fraction, and surface pressure). Air temperature and precipitation were downscaled to 0.05° using the HYDROCLIM long-term monthly climatologies of air temperature and precipitation (Hijmans et al., 2005).
- *Terrain properties* used include slope and points of the per-cell distribution of height above nearest drainage (HAND) that were derived by the authors from the global SRTM Digital Elevation Model (DEM) combined with the GTOPO30 DEM beyond 60° latitude. Flow direction was derived from the HydroSheds dataset (Lehner et al., 2008) extended with the hydro1k product beyond 60°.
- *Surface and vegetation properties* were largely derived from ESA's GlobCover version 2.2 mapping product, based on 300m resolution observations from the optical MERIS instrument between December 2004 and June 2006 (Bicheron et al., 2008). From these data, we derived

0.05° grids representing fractions of permanent water, ice and artificial surfaces, as well as fractions of deep- and shallow-rooted vegetation estimated from the land cover fractions. Vegetation height estimates were those derived from ICESat-GLAS measurements by Simard et al. (2011)

- *Snow* model parameters for the conceptual HBV were derived by Beck et al. (2016).
- *Soil properties* were derived from the GSDE dataset (Shangguan et al., 2014), a global gridded data set of soil properties. Gridded soil parameters that were derived include saturated conductivity, saturated water content, bubbling pressure and the pore size index lambda (following Brooks and Corey, 1964).
- *Aquifer properties* used include gridded estimates of shallow aquifer porosity from the GLHYMPS data set (Gleeson et al., 2014), whereas gridded estimates of groundwater recession constants were obtained from the GSDC dataset (Beck et al., 2015).

All satellite products assimilated in model run time were ultimately derived from NASA's MODIS instruments on the Aqua and Terra satellites.

- *Surface albedo and reflectance data* were derived from the combined MODIS Terra/Aqua 8-day composite products resampled to 0.05° resolution global grids (MCD43). White-sky albedo was derived from the MCD43C3.005 product, whereas percent snow cover and nadir reflectances in the red (Band 1), near infrared (Band 2), blue (Band 3) and shortwave infrared (Band 6) were obtained from the MCD43C4.005 product.
- *For leaf area index*, the MODIS GLASS product (Xiao et al., 2014) resampled to 0.05° resolution was used.
- *Land surface temperature* was derived from the MOD11C1.006 product (Wan, 2015), providing daily estimates of land surface temperature based on MODIS Terra observations resampled to daily grids. Only optimum quality data were used, indicated by a daily quality control index value of zero. Except the GLASS LAI product (downloaded from http://glcf.umd.edu/data/lai/) all satellite data were downloaded through the NASA data portal.

References

Alcamo, J., Döll, P., Henrichs, T., Kaspar, F., Lehner, B., Rösch, T., and Siebert, S.: Development and testing of the WaterGAP 2 global model of water use and availability, Hydrological Sciences Journal, 48, 317-337, 10.1623/hysj.48.3.317.45290, 2003.

Allen, R. G., Pereira, L. S., Raes, D., and Smith, M.: Crop evapotranspiration - Guidelines for computing crop water requirements., Food and Agricultural Organisation of the United Nations, Rome, 1998.

Anderson, M., Hain, C., Gao, F., Kustas, W., Yang, Y., Sun, L., Yang, Y., Holmes, T., and Dulaney, W.: Mapping evapotranspiration at multiple scales using multi-sensor data fusion, 2016 IEEE International Geoscience and Remote Sensing Symposium (IGARSS), 2016, 226-229,

Hydrol. Earth Syst. Sci. Discuss., https://doi.org/10.5194/hess-2017-757
Manuscript under review for journal Hydrol. Earth Syst. Sci.
Discussion started: 24 January 2018

Hydrology and Earth System Sciences
Open Access
Discussions

Bauer-Gottwein, P., Gondwe, B. R. N., Charvet, G., Marín, L. E., Rebolledo-Vieyra, M., and Merediz-Alonso, G.: Review: The Yucatán Peninsula karst aquifer, Mexico, Hydrogeology Journal, 19, 507-524, 10.1007/s10040-010-0699-5, 2011.

Beck, H. E., de Roo, A., and van Dijk, A. I. J. M.: Global Maps of Streamflow Characteristics Based on Observations from Several Thousand Catchments, Journal of Hydrometeorology, 16, 1478-1501, 10.1175/JHM-D-14-0155.1, 2015.

Beck, H. E., van Dijk, A. I., de Roo, A., Miralles, D. G., McVicar, T. R., Schellekens, J., and Bruijnzeel, L. A.: Global- scale regionalization of hydrologic model parameters, Water Resources Research, 2016.

Beck, H. E., van Dijk, A. I. J. M., Levizzani, V., Schellekens, J., Miralles, D. G., Martens, B., and de Roo, A.: MSWEP: 3-hourly 0.25° global gridded precipitation (1979–2015) by merging gauge, satellite, and reanalysis data, Hydrol. Earth Syst. Sci., 21, 589-615, 10.5194/hess-21-589-2017, 2017.

Bicheron, P., Defourny, P., Brockmann, C., Schouten, L., Vancutsem, C., Huc, M., Bontemps, S., Leroy, M., Achard, F., and Herold, M.: Globcover: products description and validation report, in, ME, 2008.

Bos, M. G., and Nugteren, J.: On irrigation efficiencies, 19, ILRI, 1990.

Brooks, R., and Corey, A.: Hydraulic Properties of Porous Media, of Colorado State University Hydrology Paper, 3, Colorado State University, 1964.

Dai, A., Qian, T., Trenberth, K. E., and Milliman, J. D.: Changes in continental freshwater discharge from 1948 to 2004, Journal of Climate, 22, 2773-2792, 2009.

Döll, P., and Siebert, S.: Global modeling of irrigation water requirements, Water Resources Research, 38, 2002.

Doody, T. M., Barron, O. V., Dowsley, K., Emelyanova, I., Fawcett, J., Overton, I. C., Pritchard, J. L., Van Dijk, A. I. J. M., and Warren, G.: Continental mapping of groundwater dependent ecosystems: A methodological framework to integrate diverse data and expert opinion, Journal of Hydrology: Regional Studies, 10, 61-81, http://dx.doi.org/10.1016/j.ejrh.2017.01.003, 2017.

Falkenmark, M., and Rockström, J.: Balancing water for humans and nature: the new approach in ecohydrology, Earthscan, 2004.

FAO: AQUASTAT database - Food and Agriculture Organization of the United Nations (FAO). Website accessed on 30/09/2017, in, 2017.

Frost, A. J., Ramchurn, A., and Hafeez, M.: Evaluation of the Bureau's Operational AWRA-L Model, Melbourne, 80, 2016a.

Frost, A. J., Ramchurn, A., and Smith, A. B.: The Bureau's Operational AWRA Landscape (AWRA-L) Model, Melbourne, 47, 2016b.

Gleeson, T., Moosdorf, N., Hartmann, J., and Van Beek, L. P. H.: A glimpse beneath earth's surface: GLobal HYdrogeology MaPS (GLHYMPS) of permeability and porosity, Geophysical Research Letters, 41, 3891-3898, 2014.

Glenn, E. P., Doody, T. M., Guerschman, J. P., Huete, A. R., King, E. A., McVicar, T. R., Van Dijk, A. I. J. M., Van Niel, T. G., Yebra, M., and Zhang, Y.: Actual evapotranspiration estimation by ground and remote sensing methods: the Australian experience, Hydrological Processes, 25, 4103-4116, 10.1002/hyp.8391, 2011.

Guerschman, J. P., Van Dijk, A., Mattersdorf, G., Beringer, J., Hutley, L. B., Leuning, R., Pipunic, R. C., and Sherman, B. S.: Scaling of potential evapotranspiration with MODIS data reproduces flux observations and catchment water balance observations across Australia, Journal of Hydrology, 369, 107-119, 10.1016/j.jhydrol.2009.02.013, 2009.

Hijmans, R. J., Cameron, S. E., Parra, J. L., Jones, P. G., and Jarvis, A.: Very high resolution interpolated climate surfaces for global land areas, International Journal of Climatology, 25, 1965-1978, 10.1002/joc.1276, 2005.

Holgate, C. M., De Jeu, R. A. M., van Dijk, A. I. J. M., Liu, Y. Y., Renzullo, L. J., Vinodkumar, Dharssi, I., Parinussa, R. M., Van Der Schalie, R., Gevaert, A., Walker, J., McJannet, D., Cleverly, J., Haverd, V., Trudinger, C. M., and Briggs, P. R.: Comparison of remotely sensed and modelled soil moisture data sets across Australia, Remote Sensing of Environment, 186, 479-500, http://dx.doi.org/10.1016/j.rse.2016.09.015, 2016.

Hulley, G. C., Hughes, C. G., and Hook, S. J.: Quantifying uncertainties in land surface temperature and emissivity retrievals from ASTER and MODIS thermal infrared data, Journal of Geophysical Research: Atmospheres, 117, n/a-n/a, 10.1029/2012JD018506, 2012.

Kalma, J. D., Mcvicar, T. R., and Mccabe, M. F.: Estimating land surface evaporation: a review of methods using remotely sensed surface temperature data, Surveys in Geophysics, 29, 421-469, 10.1007/s10712-008-9037-z, 2008.

Lehner, B., Verdin, K., and Jarvis, A.: New global hydrography derived from spaceborne elevation data, Eos, Transactions American Geophysical Union, 89, 93-94, 2008.

MacDonald, A. M., Bonsor, H. C., Dochartaigh, B. É. Ó., and Taylor, R. G.: Quantitative maps of groundwater resources in Africa, Environmental Research Letters, 7, 024009, 2012.

Melton, J. R., Wania, R., Hodson, E. L., Poulter, B., Ringeval, B., Spahni, R., Bohn, T., Avis, C. A., Beerling, D. J., Chen, G., Eliseev, A. V., Denisov, S. N., Hopcroft, P. O., Lettenmaier, D. P., Riley, W. J., Singarayer, J. S., Subin, Z. M., Tian, H., Zürcher, S., Brovkin, V., van Bodegom, P. M., Kleinen, T., Yu, Z. C., and Kaplan, J. O.: Present state of global wetland extent and wetland methane modelling: conclusions from a model inter-comparison project (WETCHIMP), Biogeosciences, 10, 753-788, 10.5194/bg-10-753-2013, 2013.

Miralles, D. G., Jiménez, C., Jung, M., Michel, D., Ershadi, A., McCabe, M. F., Hirschi, M., Martens, B., Dolman, A. J., Fisher, J. B., Mu, Q., Seneviratne, S. I., Wood, E. F., and Fernández-Prieto, D.: The WACMOS-ET project – Part 2: Evaluation of global terrestrial evaporation data sets, Hydrol. Earth Syst. Sci., 20, 823-842, 10.5194/hess-20-823-2016, 2016.

Nobre, A. D., Cuartas, L. A., Momo, M. R., Severo, D. L., Pinheiro, A., and Nobre, C. A.: HAND contour: a new proxy predictor of inundation extent, Hydrological Processes, 2015.

Oki, T., and Kanae, S.: Global Hydrological Cycles and World Water Resources, Science, 313, 1068-1072, 10.1126/science.1128845, 2006.

Peeters, L. J. M., Crosbie, R. S., Doble, R. C., and Van Dijk, A. I. J. M.: Conceptual evaluation of continental land-surface model behaviour, Environmental Modelling & Software, 43, 49-59, http://dx.doi.org/10.1016/j.envsoft.2013.01.007, 2013.

Portmann, F. T., Siebert, S., and Döll, P.: MIRCA2000—Global monthly irrigated and rainfed crop areas around the year 2000: A new high- resolution data set for agricultural and hydrological modeling, Global Biogeochemical Cycles, 24, 2010.

Priestley, C. H. B., and Taylor, R. J.: On the assessment of surface heat flux and evaporation using large-scale parameters, Monthly Weather Review, 100, 81-92, 1972.

Schellekens, J., Dutra, E., Martínez-de la Torre, A., Balsamo, G., van Dijk, A., Sperna Weiland, F., Minvielle, M., Calvet, J. C., Decharme, B., Eisner, S., Fink, G., Flörke, M., Peßenteiner, S., van Beek, R., Polcher, J., Beck, H., Orth, R., Calton, B., Burke, S., Dorigo, W., and Weedon, G. P.: A global water resources ensemble of hydrological models: the eartH2Observe Tier-1 dataset, Earth Syst. Sci. Data, 9, 389-413, 10.5194/essd-9-389-2017, 2017.

Shangguan, W., Dai, Y., Duan, Q., Liu, B., and Yuan, H.: A global soil data set for earth system modeling, Journal of Advances in Modeling Earth Systems, 6, 249-263, 10.1002/2013MS000293, 2014.

Siebert, S., Burke, J., Faures, J. M., Frenken, K., Hoogeveen, J., Döll, P., and Portmann, F. T.: Groundwater use for irrigation – a global inventory, Hydrol. Earth Syst. Sci., 14, 1863-1880, 10.5194/hess-14-1863-2010, 2010.

Siebert, S., and Döll, P.: Quantifying blue and green virtual water contents in global crop production as well as potential production losses without irrigation, Journal of Hydrology, 384, 198-217, 2010.

Simard, M., Pinto, N., Fisher, J. B., and Baccini, A.: Mapping forest canopy height globally with spaceborne lidar, Journal of Geophysical Research: Biogeosciences, 116, 2011.

Solley, W. B., Pierce, R. R., and Perlman, H. A.: Estimated use of water in the United States in 1995, US Geological Survey, 1998.

Thiery, W., Davin, E. L., Lawrence, D. M., Hirsch, A. L., Hauser, M., and Seneviratne, S. I.: Present-day irrigation mitigates heat extremes, Journal of Geophysical Research: Atmospheres, 122, 1403-1422, 10.1002/2016JD025740, 2017.

Thom, A. S.: Momentum, Mass and Heat Exchange of Plant Communities, in: Vegetation and the Atmosphere, edited by: Monteith, J. L., Academic Press, London, 57-109, 1975.

Tian, S., Tregoning, P., Renzullo, L. J., van Dijk, A. I. J. M., Walker, J. P., Pauwels, V. R. N., and Allgeyer, S.: Improved water balance component estimates through joint assimilation of GRACE water storage and SMOS soil moisture retrievals, Water Resources Research, 53, 1820-1840, 10.1002/2016WR019641, 2017.

Van Dijk, A. I. J. M.: AWRA Technical Report 3. Landscape Model (version 0.5) Technical Description, WIRADA / CSIRO Water for a Healthy Country Flagship, Canberra, 2010.

Van Dijk, A. I. J. M., Brakenridge, G. R., Kettner, A. J., Beck, H. E., De Groeve, T., and Schellekens, J.: River gauging at global scale using optical and passive microwave remote sensing, Water Resources Research, 52, 6404-6418, 10.1002/2015WR018545, 2016.

Van Niel, T. G., McVicar, T. R., Roderick, M. L., van Dijk, A. I. J. M., Renzullo, L. J., and van Gorsel, E.: Correcting for systematic error in satellite-derived latent heat flux due to assumptions in temporal scaling: Assessment from flux tower observations, Journal of Hydrology, 409, 140-148, 10.1016/j.jhydrol.2011.08.011, 2011.

Wada, Y., Wisser, D., and Bierkens, M. F. P.: Global modeling of withdrawal, allocation and consumptive use of surface water and groundwater resources, Earth System Dynamics, 5, 15-40, 2014.

Wan, Z., Zhang, Y., Zhang, Q., and Li, Z. L.: Quality assessment and validation of the MODIS global land surface temperature, International Journal of Remote Sensing, 25, 261-274, 10.1080/0143116031000116417, 2004.

Wan, Z.: New refinements and validation of the MODIS Land-Surface Temperature/Emissivity products, Remote Sensing of Environment, 112, 59-74, 2008.

Wan, Z., and Li, Z. L.: Radiance- based validation of the V5 MODIS land- surface temperature product, International Journal of Remote Sensing, 29, 5373-5395, 10.1080/01431160802036565, 2008.

Wan, Z.: MOD11C1 MODIS/Terra Land Surface Temperature/Emissivity Daily L3 Global 0.05Deg CMG V006. , in, edited by: (https://doi.org/10.5067/modis/mod11c1.006), N. E. L. P. D., 2015.

Wang-Erlandsson, L., Bastiaanssen, W. G., Senay, G. B., van Dijk, A. I., Guerschman, J. P., Keys, P. W., Gordon, L. J., and Savenije, H. H.: Global root zone storage capacity from satellite-based evaporation, Hydrology and Earth System Sciences, 20, 1459, 2016.

Weedon, G. P., Balsamo, G., Bellouin, N., Gomes, S., Best, M. J., and Viterbo, P.: The WFDEI meteorological forcing data set: WATCH Forcing Data methodology applied to ERA- Interim reanalysis data, Water Resources Research, 50, 7505-7514, 2014.

Wood, E. F., Roundy, J. K., Troy, T. J., van Beek, L. P. H., Bierkens, M. F. P., Blyth, E., de Roo, A., Döll, P., Ek, M., Famiglietti, J., Gochis, D., van de Giesen, N., Houser, P., Jaffé, P. R., Kollet, S., Lehner, B., Lettenmaier, D. P., Peters-Lidard, C., Sivapalan, M., Sheffield, J., Wade, A., and Whitehead, P.: Hyperresolution global land surface modeling: Meeting a grand challenge for monitoring Earth's terrestrial water, Water Resources Research, 47, W05301, 10.1029/2010WR010090, 2011.

Xiao, Z., Liang, S., Wang, J., Chen, P., Yin, X., Zhang, L., and Song, J.: Use of general regression neural networks for generating the GLASS leaf area index product from time-series MODIS surface reflectance, IEEE Transactions on Geoscience and Remote Sensing, 52, 209-223, 2014.

Yebra, M., Van Dijk, A., Leuning, R., Huete, A., and Guerschman, J. P.: Evaluation of optical remote sensing to estimate actual evapotranspiration and canopy conductance, Remote Sensing of Environment, 129, 250-261, 2013.

Yebra, M., Van Dijk, A. I., Leuning, R., and Guerschman, J. P.: Global vegetation gross primary production estimation using satellite-derived light-use efficiency and canopy conductance, Remote Sensing of Environment, 163, 206-216, 2015.

Zhang, Y., Peña-Arancibia, J. L., McVicar, T. R., Chiew, F. H., Vaze, J., Liu, C., Lu, X., Zheng, H., Wang, Y., and Liu, Y. Y.: Multi-decadal trends in global terrestrial evapotranspiration and its components, Scientific reports, 6, 19124, 2016.